Check for updates

Rydberg excitons in Cu_2O microcrystals grown on a silicon platform

Stephan Steinhauer [1 ✉], Marijn A.M. Versteegh[1], Samuel Gyger [1], Ali W. Elshaari [1], Birgit Kunert[2], André Mysyrowicz[3] & Val Zwiller[1]

Cuprous oxide (Cu_2O) is a semiconductor with large exciton binding energy and significant technological importance in applications such as photovoltaics and solar water splitting. It is also a superior material system for quantum optics that enabled the observation of intriguing phenomena, such as Rydberg excitons as solid-state analogue to highly-excited atomic states. Previous experiments related to excitonic properties focused on natural bulk crystals due to major difficulties in growing high-quality synthetic samples. Here, the growth of Cu_2O microcrystals with excellent optical material quality and very low point defect levels is presented. A scalable thermal oxidation process is used that is ideally suited for integration on silicon, demonstrated by on-chip waveguide-coupled Cu_2O microcrystals. Moreover, Rydberg excitons in site-controlled Cu_2O microstructures are shown, relevant for applications in quantum photonics. This work paves the way for the wide-spread use of Cu_2O in optoelectronics and for the development of novel device technologies.

[1] Department of Applied Physics, KTH Royal Institute of Technology, SE-106 91 Stockholm, Sweden. [2] Institute of Solid State Physics, Graz University of Technology, A-8010 Graz, Austria. [3] Laboratoire d'Optique Appliquée, ENSTA, CNRS, Ecole Polytechnique, F-91762 Palaiseau, France. ✉email: ssteinh@kth.se

Light-matter interactions in the direct-band-gap semi-conductor cuprous oxide (Cu_2O) are widely governed by excitons, quasi-particles arising from electron-hole Coulomb interactions, which can be observed up to room temperature due to their large binding energy. As a result of the unique excitonic properties, intriguing condensed-matter quantum phenomena have been demonstrated, e.g. spectroscopic signatures of quantum-degenerate exciton gases[1,2] as well as giant Rydberg excitons[3] exhibiting signatures of quantum coherences[4] and quantum chaotic behavior[5]. As the exciton ground state – the so-called paraexciton – is decoupled from the radiation field in unstrained Cu_2O, paraexcitons can reach lifetimes up to micro-seconds[6] rendering them a prime candidate for excitonic Bose-Einstein condensation[7]. Apart from quantum optics, recent reports have reinforced the significant potential of Cu_2O as a low-cost, non-toxic material in areas such as photocatalysis[8], solar water splitting[9], and solar cell devices[10] showing promising photovoltaic efficiencies and marked excitonic effects[11]. Various methods have been reported for the growth of Cu_2O thin films and single crystals[12], in particular molecular beam epitaxy[13,14], magnetron sputtering[15,16] in combination with thermal anneal-ing[17], electrodeposition[18], thermal oxidation[19], and the floating zone method[20]. However, state-of-the-art quantum optics experiments still focus on natural bulk crystals originating from mines, clearly underlining that significant progress in Cu_2O growth is required to surpass inherent limitations of natural samples. Recent literature emphasized that for the observation of Rydberg states with principal quantum numbers higher than the current record value of $n = 25$ samples with lower impurity concentrations are required[21]. In addition, scalable fabrication techniques suitable for obtaining micro-/nanostructures and compatible with standard silicon processing are needed to deploy the full potential of this material in advanced device technologies, for instance integrated quantum photonic circuits.

In this work, we present Cu_2O growth by a scalable thermal oxidation process, which resulted in microcrystal structures with very low point defect and impurity levels. Our method offers the opportunity for combining high-quality Cu_2O with silicon-based integrated photonics, which we demonstrate by on-chip coupling of exciton luminescence to a silicon nitride waveguide. In single Cu_2O microcrystals studied at cryogenic temperatures under continuous-wave excitation we demonstrate luminescence from excited np Rydberg states in lithographically site-controlled structures, exhibiting excellent agreement with a hydrogen-like quantum number dependence. Due to the exceptional optical material quality and the unique excitonic properties, our Cu_2O microcrystals are highly promising for enabling new integrated photonic device architectures relevant for quantum information processing and quantum sensing.

Results and discussion

Growth and photoluminescence properties.
The growth of Cu_2O microcrystals relied on a scalable single-step thermal oxi-dation process schematically depicted in Fig. 1a. Copper films (thickness ~700 nm) were deposited by electron beam evapora-tion on silicon substrates covered with a thermal SiO_2 layer. Thermal oxidation in a tube furnace resulted in Cu_2O films with microcrystalline morphology, which can be seen in the top-view and cross-sectional scanning electron microscopy images. The Cu_2O microcrystals showed terrace-like structures on the surface (Supplementary Fig. 1) and faceted grains with sizes in the μm range. As-deposited copper and samples after thermal oxidation to Cu_2O were characterized by X-ray diffraction (XRD) mea-surements (Fig. 1b) to determine their phase composition. For as-deposited copper, the expected face-centered cubic structure and

texturing along the [111] direction was found. The presented single-step thermal oxidation method resulted in phase-pure Cu_2O with cubic cuprite structure. For samples fabricated with different growth conditions comparable microcrystal morphology as well as similar XRD results were obtained (Supplementary Fig. 2).

Thermal oxidation of copper can lead to different oxide phases[12]; Cu_2O growth was reported to proceed via the random nucleation of islands, which exhibit a cube-on-cube epitaxial relationship at the metal-oxide interface (low oxygen partial pressures)[22] or non-epitaxial orientations (above critical oxygen partial pressures depending on the copper surface)[23]. For the range of experimental parameters corresponding to the growth conditions used in this study (800–850 °C, p ~1 mbar of synthetic air) the initial stages of copper oxidation include epitaxial oxide formation accompanied by rapid two-dimensional growth[24]. The XRD results before and after thermal oxidation (Fig. 1b) show pronounced texturing in {111} direction in both cases, indicating that the oxidation proceeds via an epitaxial relationship of Cu_2O {111} || Cu {111}. This relationship is in accordance with literature reports on the thermal oxidation of copper thin films[22] and nanoparticles with sizes down to few nanometers[25]. Similar to a previous report on epitaxial Cu_2O growth on MgO[15], the observed terrace-like structures on the Cu_2O surfaces are suggesting a two-dimensional growth mode for individual microcrystals.

In addition to growth on planar silicon substrates covered with thermal SiO_2, we show the integration of Cu_2O microcrystals with pre-patterned silicon nitride waveguides (see Methods section). Site-controlled microstructures were obtained by thermal oxida-tion of lithographically defined copper rectangles (length 20 μm, width 10 μm) using the same parameters as described above. The optical material quality was assessed by means of room-temperature photoluminescence spectroscopy of Cu_2O grown on both planar substrates and on waveguide structures. In the latter case, waveguide-coupled Cu_2O luminescence was collected from the cleaved silicon nitride side facet (see experimental setup in Supplementary Fig. 3). Distinct free exciton emission was observed (Fig. 1c) for both types of samples, exhibiting a characteristic lineshape resulting from multiple phonon-assisted recombination processes with spectral overlap[13]. At photon energies attributed to copper vacancies or single/double-charged oxygen vacancies[12] no marked luminescence was observed. Additional data for microcrystalline Cu_2O films from different batches and grown under different conditions can be found in Supplementary Fig. 4, which shows spectra with very similar characteristics. Hence, the presented single-step thermal oxida-tion process is a robust method for the realization of microcrystalline Cu_2O films with very low point defect levels, ideally suited for the on-chip integration with waveguide structures. Compared to previous literature reports on Cu_2O growth on silicon (e.g. refs. [16–18]), our results demonstrate a unique combination of excellent optical material quality, site-controlled growth and suitability for photonic circuit integration, which holds great promise for enabling integrated devices with novel functionalities based on excitons in Cu_2O. In the following, we will focus on photoluminescence spectroscopy of single Cu_2O microcrystals at milli-Kelvin temperatures to probe their funda-mental excitonic properties.

Point defects and yellow 1s excitons.
Local deviations from the ideal cuprite crystalline structure, e.g. vacancy point defects, extrinsic impurities or microscopic strain, have a significant impact on the relaxation of excitons in Cu_2O and the related photon emission. Low point defect densities are highly important
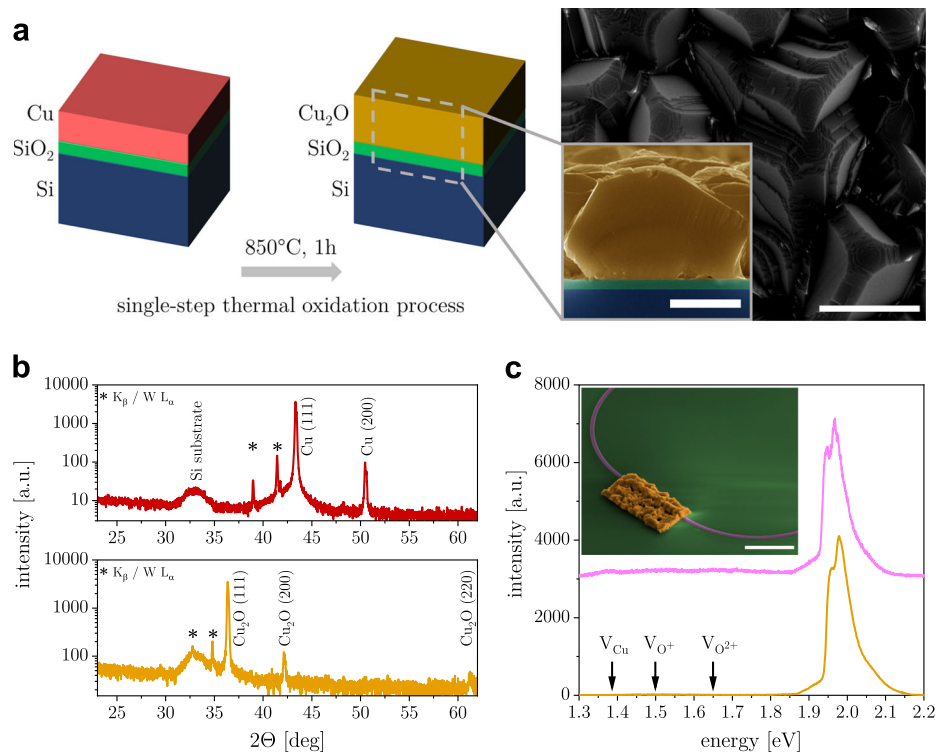
Fig. 1 Growth and characterization of Cu$_2$O microcrystals. a Schematics of sample layer structure before and after the thermal oxidation process (left). Top-view scanning electron micrograph of Cu$_2$O microcrystals after thermal oxidation at 850°C for 1 h at pressures of 1 mbar synthetic air (right); the bottom inset shows a corresponding cross-sectional image (scale bars 1 μm). **b** X-ray diffraction of as-deposited copper film (top) and Cu$_2$O film after thermal oxidation (bottom). **c** Room-temperature photoluminescence spectroscopy of Cu$_2$O microcrystals under continuous-wave laser excitation (532 nm). Emission from free exciton recombination around 2 eV was observed from Cu$_2$O microcrystals in continuous films on SiO$_2$ (bottom orange line). Further, Cu$_2$O microstructures were grown on silicon nitride waveguides (device configuration shown in the inset; scale bar 10 μm) and on-chip coupling was demonstrated by collecting the exciton emission from the cleaved waveguide side facet (top magenta line).

for efficient cooling of the exciton gas in Cu$_2$O as trapping at defects is a limiting factor for exciton lifetimes. The latter were found to be significantly shortened for increasing oxygen vacancy concentrations[26]. Furthermore, it has been suggested that relaxation processes involving vacancies can lead to heating due to phonon emission[27], which is detrimental for achieving cold exciton gas temperatures. Photoluminescence spectroscopy experiments were conducted in a dilution refrigerator (sample stage base temperature around 40 mK) to assess the optical material quality of Cu$_2$O microcrystals at milli-Kelvin temperatures. The results were compared to natural bulk Cu$_2$O as benchmark (crystal originates from a selected high-quality geological sample used in previous literature[1,2,6]). Spectra normalized to the yellow 1**s** orthoexciton emission that were acquired at a laser power of 50 μW (corresponding to a peak intensity of 3 kW cm^{-2}) and an excitation wavelength of 532 nm are presented in Fig. 2a, showing considerably reduced emission related to oxygen vacancies for the case of Cu$_2$O microcrystals. An emission feature around 1.95 eV was observed for both Cu$_2$O microcrystals and the natural bulk sample, which has been reported repeatedly in literature. It was attributed to phonon-assisted transitions and defect emission in close spectral proximity[14,27,28] with the latter potentially being correlated with local strain in the sample[29]. The ratio of excitonic over defect emission for the measurements shown in Fig. 2a was found to be about five times higher for the Cu$_2$O microcrystals compared to the bulk sample. Additional data for different samples and natural bulk crystal positions as well as further discussion can be found in Supplementary Fig. 5. In addition to intrinsic point defects,

excitons and their luminescence properties may be influenced by the presence of extrinsic impurities. The latter can lead to the formation of bound excitons, which show multiple emission lines in the energy range around ~2.00 eV, below the phonon-assisted orthoexciton transition[30]. In Fig. 2b, we directly compare photoluminescence spectra obtained from synthetic Cu$_2$O microcrystals and from the natural bulk crystal under identical experimental conditions (excitation power 50 nW). It is evident that all peak-like features related to excitons bound to extrinsic impurities are absent in Cu$_2$O microcrystals, once more validating the excellent purity and material quality of our samples. Moreover, we assess the energy level structure of yellow 1**s** excitons in Cu$_2$O microcrystals by monitoring luminescence from different phonon-assisted transitions (Fig. 2c). The emission features were assigned according to previous literature[31] and the energy splitting of 1**s** excitons into orthoexcitons and paraexcitons separated by 12 meV in unstrained Cu$_2$O was validated. The influence of strain on the luminescence spectra of Cu$_2$O microcrystals is discussed in Supplementary Fig. 6.

Exciton relaxation was further studied by assessing its excitation power dependence. For this purpose, the incident laser power was varied and the luminescence spectra were integrated in an energy range covering bound excitons, phonon-assisted transitions and the direct quadrupole line (Fig. 2d). The integrated intensity of the Cu$_2$O microcrystal is in excellent agreement with a linear relationship (slope 0.995 ± 0.008) for excitation powers spanning more than two orders of magnitude, showing slight sub-linear behavior at elevated excitation levels. On the other hand, deviations from a linear power dependence
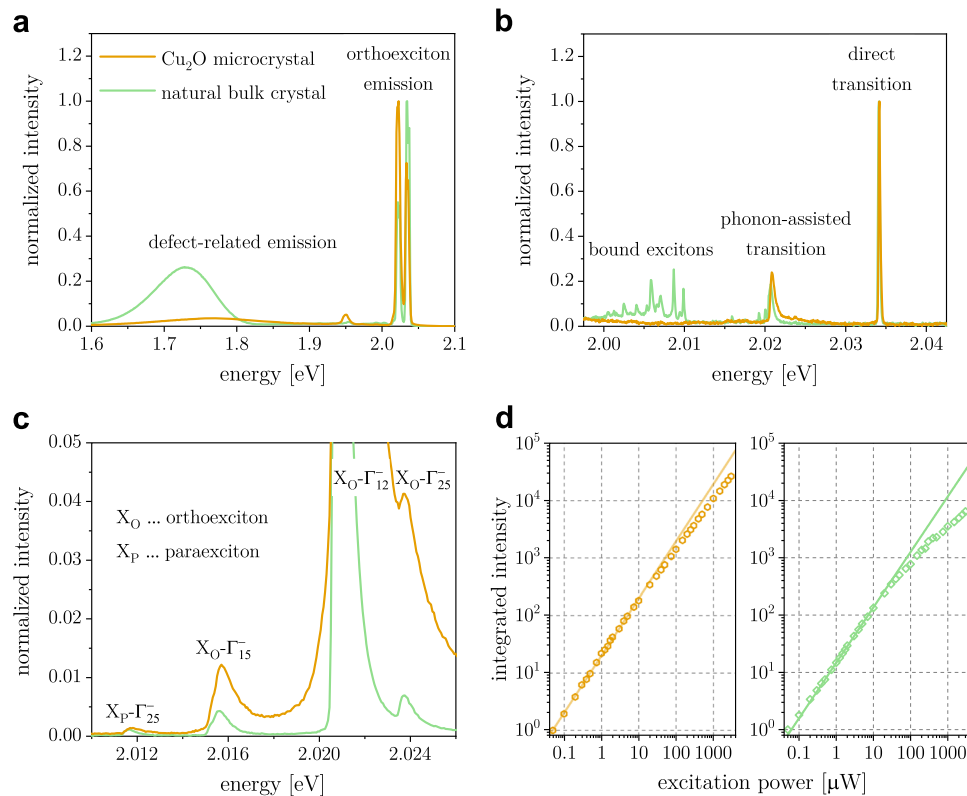
Fig. 2 Photoluminescence spectroscopy of Cu₂O microcrystals at milli-Kelvin temperatures benchmarked to measurements on a natural bulk crystal.
a Normalized photoluminescence of excitons and point defects (excitation power 50 μW). **b** Normalized emission from different excitonic transitions and bound excitons at low excitation power of 50 nW. **c** Phonon-assisted transitions of ortho- and paraexcitons (spectra normalized to direct transition; excitation power 50 μW). **d** Excitation power dependence of integrated emission in an energy range covering bound excitons, phonon-assisted transitions and the direct quadrupole line. Solid lines are a linear fit (Cu₂O microcrystal, left) and a linear curve as guide to the eye (natural bulk crystal, right), respectively.

were significantly more pronounced for the natural bulk crystal. Sub-linear power dependence of excitonic emissions in Cu₂O has been previously observed in experiments using natural bulk samples[30,32,33] and synthetic crystals grown by the floating zone method[34] using various types of laser excitation. It has been attributed to an efficient non-radiative two-body recombination process, which can be explained by Auger decay[35], by the formation of short-lived biexcitons[36] or by exciton interconversion via spin exchange[37]. The estimated recombination rates reported in literature vary considerably as the process is expected to be sensitive to Cu₂O crystal symmetry and the resulting band structure; hence it has been anticipated that Auger recombination is associated with broken band symmetries in the vicinity of impurities[7], which would explain the less pronounced two-body decay in low-defect-density Cu₂O microcrystals.

Rydberg excitons of the yellow *np* series. After initial experiments in the middle of the last century, Rydberg excitons in Cu₂O have recently attracted considerable attention due to the experimental demonstration of principal quantum numbers up to $n = 25$ in absorption measurements using natural bulk crystals[3]. For synthetic Cu₂O films in the thickness range of few micrometers and below, Rydberg excitons up to $n = 4$ have been found[38,39]. Previous studies on natural bulk Cu₂O crystals indicated that under above-band excitation Rydberg excitons are generated via collision processes of 1s excitons[28,40]. The question arises if Rydberg states can also be observed in the Cu₂O microcrystals presented here, which was assessed by means of

photoluminescence experiments. Results obtained for varying incident laser powers are presented in Fig. 3a (spectra normalized to their respective maxima). Emission peaks corresponding to Rydberg excitons up to $n = 6$ were identified at intermediate excitation, which can also be seen in the exemplary spectrum shown in Fig. 3b. The 2p peak showed a markedly asymmetric lineshape consistent with previous literature on bulk Cu₂O crystals[28,40,41], whereas the relative emission intensities from *np* states differed in our case. The minor peak between the 2p and 3p energy level is attributed to 1s excitons of the green series[28]. Rydberg exciton emission showed broadening for increasing excitation power, which can be explained by a combination of phonon scattering and density-dependent effects[40]; the red shift indicates a bandgap decrease due to laser-induced sample heating. Most importantly, the power-dependent measurements verify the robustness of Rydberg excitons in Cu₂O microcrystals as their emission was detected in a wide range of excitation conditions. To reduce the line broadening, measurements were performed at considerably lower excitation powers. The spectral overlap of states with higher quantum numbers could be reduced and the observation of Rydberg excitons with $n = 7$ was possible, which is further detailed in Supplementary Fig. 7 and the related discussion. Additional photoluminescence spectroscopy data from different samples is shown in Supplementary Fig. 8, validating that Rydberg excitons can be consistently observed in Cu₂O microcrystals.

Furthermore, site-controlled Cu₂O microstructures (Fig. 3c) were achieved by lithographic patterning of the copper film before oxidation. We demonstrate luminescence from excited
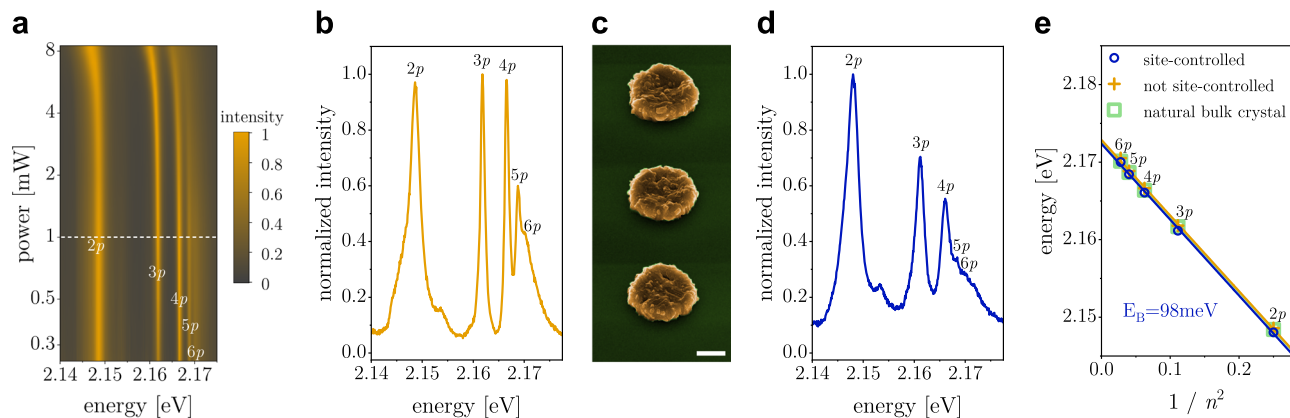
Fig. 3 Rydberg excitons in Cu₂O microcrystals and site-controlled structures. a Normalized photoluminescence of np Rydberg exciton emission from Cu₂O microcrystal for varying excitation powers. The white dashed line indicates the spectrum presented in **b** which was acquired at an excitation power of 1 mW and a cryostat stage temperature around 1.8 K. **c** Scanning electron micrograph of site-controlled circular Cu₂O microstructures with 5 µm diameter (scale bar 2 µm; sample tilt 45°). **d** Photoluminescence spectrum of site-controlled Cu₂O microstructure that was acquired under identical experimental conditions as in **b**. **e** Rydberg exciton energies as a function of n^{-2} and the corresponding linear fits to extract the exciton binding energy E_B.

Rydberg states in a circular Cu₂O microstructure with 5µm diameter (Fig. 3d). The intensity ratio of np states was different compared to Cu₂O microcrystals, which could be explained by variations in microscopic strain[41]. The Rydberg exciton energies were evaluated as a function of n^{-2} for results obtained from site-controlled microstructures, from not site-controlled microcrystals and from a natural bulk crystal (Fig. 3e). Excellent agreement with a linear relation was found and exciton binding energies of 98 meV and 97 meV were deduced for the synthetic samples and the natural bulk crystal, respectively. The extracted exciton binding energies concur with previous findings using bulk crystals, obtained from both photoluminescence (97 meV[40]; 98.5 meV[41]) and absorption measurements (98 meV[42]). Hence our results demonstrate the realization of site-controlled, micrometer-sized Cu₂O structures as host platform for Rydberg excitons, which goes beyond the state of the art of Cu₂O growth on silicon and opens up opportunities for unprecedented photonic device architectures. For instance, our technology will enable applications in nonlinear quantum optics relying on interactions between Rydberg states[43], as clear signatures of the Rydberg blockade effect have been recently reported for principal quantum numbers around $n = 6$[21]. To observe Rydberg states with higher principal quantum number n, it will be promising to explore Cu₂O microcrystals with larger size as well as different excitation schemes that mitigate luminescence broadening[40] and the potential influence of free carriers induced by above-band excitation[21].

In summary, we have presented the growth of Cu₂O microcrystals showing excellent optical material quality with very low point defect and impurity levels, combined with the integration on a silicon platform including the on-chip coupling to silicon nitride waveguide structures. The fabrication method for obtaining high-quality Cu₂O films via a scalable thermal oxidation process has guiding significance for diverse areas where this low-cost, non-toxic material is employed, such as photovoltaics and photocatalysis. Furthermore, the demonstration of Rydberg excitons in Cu₂O microcrystals and their integration on silicon have far-reaching implications for future applications in photonic quantum information processing. For instance, Rydberg states in Cu₂O have been proposed for the realization of novel solid-state single-photon sources[44] and giant optical nonlinearities[45]. Hence our work lays the foundation for a platform technology enabling solid-state Rydberg excitations on-chip,

which is envisioned to result in integrated devices capable of generating and manipulating light at the single-photon level.

Methods

Growth of Cu₂O microcrystals on silicon substrates. The deposition of copper films (thickness ~700 nm) was performed by electron beam evaporation onto pieces of silicon wafers with 150 nm thermal SiO₂. A thin intermediate titanium layer (thickness ~5 nm) was employed to improve the film adhesion on the substrate surface. Samples with structured Cu₂O were realized by patterning the copper film using an electron beam lithography lift-off process. Thermal oxidation was carried out in a tube furnace connected to a vacuum pump. Before growth experiments the system was evacuated and purged multiple times using high-purity synthetic air (Air Liquide Alphagaz 2). Cu₂O samples were grown by thermal oxidation at a pressure around 1 mbar and setpoint temperatures of 800 °C or 850 °C. The temperature was kept constant for 1 h or 5 h after reaching the setpoint value, followed by natural sample cool-down.

Sample characterization. The morphologies of Cu₂O films and microstructures were characterized by scanning electron microscopy imaging of the sample surfaces and of cross-sections obtained by mechanical cleaving. X-ray diffraction measurements were performed by specular scans using a PANalytical Empyrean system. Radiation from a sealed copper tube was used in combination with a secondary graphite monochromator in Bragg-Brentano geometry. Phase analysis was carried out relying on powder patterns from the database PDF2, International Center for Diffraction Data, using 004-0836 for Cu and 005-0667 for Cu₂O.

Photoluminescence spectroscopy. All photoluminescence spectroscopy experiments were performed using a Horiba iHR550 spectrometer and a continuous-wave, diode-pumped solid-state laser emitting at 532 nm. Room-temperature spectra were acquired using an objective (NA = 0.82) for excitation and collection. Spectroscopy at milli-Kelvin temperatures was performed relying on a cryogen-free dilution refrigerator (Bluefors) with a base temperature around 10 mK. Optical side-access windows with anti-reflective coatings were used for laser excitation of the samples mounted on a dedicated stage controlled by piezoelectric actuators, which had a base temperature around 40 mK. The laser was focused by a lens (NA = 0.50) inside the cryostat to a spot diameter around 1.2 µm (full width at half maximum); the power was measured at the outermost cryostat window.

Waveguide integration of Cu₂O microstructures. Commercial silicon wafers covered with 3.3 µm wet thermal oxide and 335 nm of stoichiometric silicon nitride deposited by low-pressure chemical vapor deposition were used as substrates. Waveguides with a width of 1 µm were fabricated using electron beam lithography and reactive ion etching using CHF₃/CF₄/O₂ gas chemistry. Integrated Cu₂O microstructures were realized by an electron beam lithography lift-off process and thermal oxidation at 850 °C for 1 h. Photoluminescence spectroscopy of the waveguide-integrated device was performed using an Acton SpectraPro spectrometer with 750 mm focal length, excitation normal to the sample surface (continuous-wave 532 nm laser) through an objective (NA = 0.28) and collection from the cleaved waveguide facet using another objective (NA = 0.65).

Data availability

References

1. Snoke, D., Wolfe, J. P. & Mysyrowicz, A. Quantum saturation of a Bose gas: excitons in Cu_2O. *Phys. Rev. Lett.* **59**, 827–830 (1987).
2. Snoke, D. W., Wolfe, J. P. & Mysyrowicz, A. Evidence for Bose-Einstein condensation of a two-component exciton gas. *Phys. Rev. Lett.* **64**, 2543–2546 (1990).
3. Kazimierczuk, T., Fröhlich, D., Scheel, S., Stolz, H. & Bayer, M. Giant Rydberg excitons in the copper oxide Cu_2O. *Nature* **514**, 343–347 (2014).
4. Grünwald, P. et al. Signatures of quantum coherences in Rydberg excitons. *Phys. Rev. Lett.* **117**, 133003 (2016).
5. Aßmann, M., Thewes, J., Fröhlich, D. & Bayer, M. Quantum chaos and breaking of all anti-unitary symmetries in Rydberg excitons. *Nat. Mater.* **15**, 741–745 (2016).
6. Mysyrowicz, A., Hulin, D. & Antonetti, A. Long exciton lifetime in Cu_2O. *Phys. Rev. Lett.* **43**, 1123–1126 (1979).
7. Snoke, D. & Kavoulakis, G. M. Bose-Einstein condensation of excitons in Cu_2O: progress over 30 years. *Rep. Prog. Phys.* **77**, 116501 (2014).
8. Wu, S.-C., Tan, C.-S. & Huang, M. H. Strong facet effects on interfacial charge transfer revealed through the examination of photocatalytic activities of various Cu_2O-ZnO heterostructures. *Adv. Funct. Mater.* **27**, 1604635 (2017).
9. Pan, L. et al. Boosting the performance of Cu_2O photocathodes for unassisted solar water splitting devices. *Nat. Catal.* **1**, 412–420 (2018).
10. Minami, T., Nishi, Y. & Miyata, T. Efficiency enhancement using a $Zn_{1−x}Ge_x$-O thin film as an n-type window layer in Cu_2O-based heterojunction solar cells. *Appl. Phys. Express* **9**, 052301 (2016).
11. Omelchenko, S. T., Tolstova, Y., Atwater, H. A. & Lewis, N. S. Excitonic effects in emerging photovoltaic materials: a case study in Cu_2O. *ACS Energy Lett.* **2**, 431–437 (2017).
12. Meyer, B. K. et al. Binary copper oxide semiconductors: from materials towards devices. *Phys. Stat. Sol. (B)* **249**, 1487–1509 (2012).
13. Li, J. et al. Engineering of optically defect free Cu_2O enabling exciton luminescence at room temperature. *Opt. Mater. Express* **3**, 2072–2077 (2013).
14. Kracht, M., Schörmann, J. & Eickhoff, M. Plasma assisted molecular beam epitaxy of Cu_2O on MgO(001): influence of copper flux on epitaxial orientation. *J. Cryst. Growth* **436**, 87–91 (2016).
15. Yin, Z. G. et al. Two-dimensional growth of continuous Cu_2O thin films by magnetron sputtering. *Appl. Phys. Lett.* **86**, 061901 (2005).
16. Park, J.-W. et al. Microstructure, optical property, and electronic band structure of cuprous oxide thin films. *J. Appl. Phys.* **110**, 103503 (2011).
17. Bergum, K. et al. Improving carrier transport in Cu_2O thin films by rapid thermal annealing. *J. Phys. Condens. Matter* **30**, 075702 (2018).
18. Oba, F. et al. Epitaxial growth of cuprous oxide electrodeposited onto semiconductor and metal substrates. *J. Am. Ceram. Soc.* **88**, 253–270 (2005).
19. Mani, S., Jang, J., Ketterson, J. & Park, H. High-quality Cu_2O crystals with various morphologies grown by thermal oxidation. *J. Cryst. Growth* **311**, 3549–3552 (2009).
20. Chang, K. B., Frazer, L., Schwartz, J. J., Ketterson, J. B. & Poeppelmeier, K. R. Removal of copper vacancies in cuprous oxide single crystals grown by the floating zone method. *Cryst. Growth Des.* **13**, 4914–4922 (2013).
21. Heckötter, J. et al. Rydberg excitons in the presence of an ultralow-density electron-hole plasma. *Phys. Rev. Lett.* **121**, 097401 (2018).
22. Zhou, G. et al. In situ atomic-scale visualization of oxide islanding during oxidation of Cu surfaces. *Chem. Commun.* **49**, 10862–10864 (2013).
23. Luo, L., Kang, Y., Yang, J. C. & Zhou, G. Effect of oxygen gas pressure on orientations of Cu_2O nuclei during the initial oxidation of Cu(100), (110) and (111). *Surf. Sci.* **606**, 1790–1797 (2012).
24. Gattinoni, C. & Michaelides, A. Atomistic details of oxide surfaces and surface oxidation: the example of copper and its oxides. *Surf. Sci. Rep.* **70**, 424–447 (2015).
25. LaGrow, A. P., Ward, M. R., Lloyd, D. C., Gai, P. L. & Boyes, E. D. Visualizing the Cu/Cu_2O interface transition in nanoparticles with environmental scanning transmission electron microscopy. *J. Am. Chem. Soc.* **139**, 179–185 (2017).
26. Koirala, S., Naka, N. & Tanaka, K. Correlated lifetimes of free paraexcitons and excitons trapped at oxygen vacancies in cuprous oxide. *J. Lumin.* **134**, 524–527 (2013).
27. Frazer, L., Chang, K. B., Schaller, R. D., Poeppelmeier, K. R. & Ketterson, J. B. Vacancy relaxation in cuprous oxide ($Cu_{2−x}O_{1−y}$). *J. Lumin.* **183**, 281–290 (2017).
28. Takahata, M. & Naka, N. Photoluminescence properties of the entire excitonic series in Cu_2O. *Phys. Rev. B* **98**, 195205 (2018).
29. Frazer, L. et al. Evaluation of defects in cuprous oxide through exciton luminescence imaging. *J. Lumin.* **159**, 294–302 (2015).
30. Jang, J. I., Sun, Y., Watkins, B. & Ketterson, J. B. Bound excitons in Cu_2O: Efficient internal free exciton detector. *Phys. Rev. B* **74**, 235204 (2006).
31. Mysyrowicz, A., Trauernicht, D. P., Wolfe, J. P. & Trebin, H. R. Stress dependence of the paraexciton in Cu_2O. *Phys. Rev. B* **27**, 2562–2564 (1983).
32. O'Hara, K. E., Gullingsrud, J. R. & Wolfe, J. P. Auger decay of excitons in Cu_2O. *Phys. Rev. B* **60**, 10872–10885 (1999).
33. Stolz, H. et al. Condensation of excitons in Cu_2O at ultracold temperatures: experiment and theory. *New J. Phys.* **14**, 105007 (2012).
34. Karpinska, K., Mostovoy, M., van der Vegte, M. A., Revcolevschi, A. & van Loosdrecht, P. H. M. Decay and coherence of two-photon excited yellow orthoexcitons in Cu_2O. *Phys. Rev. B* **72**, 155201 (2005).
35. Wolfe, J. P. & Jang, J. I. The search for Bose-Einstein condensation of excitons in Cu_2O: exciton-Auger recombination versus biexciton formation. *New J. Phys.* **16**, 123048 (2014).
36. Jang, J. I. & Wolfe, J. P. Auger recombination and biexcitons in Cu_2O: A case for dark excitonic matter. *Phys. Rev. B* **74**, 045211 (2006).
37. Kavoulakis, G. M. & Mysyrowicz, A. Auger decay, spin exchange, and their connection to Bose-Einstein condensation of excitons in Cu_2O. *Phys. Rev. B* **61**, 16619–16622 (2000).
38. Naka, N., Hashimoto, S. & Ishihara, T. Thin films of single-crystal cuprous oxide grown from the melt. *Jpn J. Appl. Phys.* **44**, 5096–5101 (2005).
39. Takahata, M., Tanaka, K. & Naka, N. Nonlocal optical response of weakly confined excitons in Cu_2O mesoscopic films. *Phys. Rev. B* **97**, 205305 (2018).
40. Kitamura, T., Takahata, M. & Naka, N. Quantum number dependence of the photoluminescence broadening of excitonic Rydberg states in cuprous oxide. *J. Lumin.* **192**, 808–813 (2017).
41. Reimann, K. & Syassen, K. Raman scattering and photoluminescence in Cu_2O under hydrostatic pressure. *Phys. Rev. B* **39**, 11113–11119 (1989).
42. Matsumoto, H., Saito, K., Hasuo, M., Kono, S. & Nagasawa, N. Revived interest on yellow-exciton series in Cu_2O: an experimental aspect. *Solid State Commun.* **97**, 125–129 (1996).
43. Firstenberg, O., Adams, C. S. & Hofferberth, S. Nonlinear quantum optics mediated by Rydberg interactions. *J. Phys. B At. Mol. Opt. Phys.* **49**, 152003 (2016).
44. Khazali, M., Heshami, K. & Simon, C. Single-photon source based on Rydberg exciton blockade. *J. Phys. B At. Mol. Opt. Phys.* **50**, 215301 (2017).
45. Walther, V., Johne, R. & Pohl, T. Giant optical nonlinearities from Rydberg excitons in semiconductor microcavities. *Nat. Commun.* **9**, 1309 (2018).

Acknowledgements

Author contributions

S.S., M.A.M.V., and V.Z. conceived the experiments, with input from A.M. M.A.M.V. designed and built the milli-Kelvin photoluminescence spectroscopy setup. S.S. performed material growth, SEM characterization and photoluminescence experiments. S.G. and A.W.E. fabricated and characterized waveguide-integrated structures. Data analysis and interpretation was performed by S.S. with support from M.A.M.V., A.M., and V.Z. XRD characterization and the corresponding analysis was performed by B.K. The project was supervised by M.A.M.V. and V.Z. The manuscript was written by S.S. with inputs from all authors.

Competing interests

The authors declare no competing interests.

Additional information

Supplementary information is available for this paper at https://doi.org/10.1038/s43246-020-0013-6.

Correspondence and requests for materials should be addressed to S.S.

Reprints and permission information is available at http://www.nature.com/reprints

Publisher's note Springer Nature remains neutral with regard to jurisdictional claims in published maps and institutional affiliations.